Engineering xxx (xxxx) xxx

Contents lists available at ScienceDirect

Engineering

journal homepage: www.elsevier.com/locate/eng

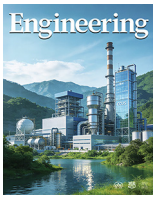

Research
Antimicrobial Resistance—Article

Boosting Fosfomycin Efficacy Against Methicillin-Resistant *Staphylococcus aureus* Infections by Targeting Pyrimidine Metabolism

Jianya Luo [a], Qingyan Lv [a], Mengping He [a], Zhiqiang Wang [a,b], Yuan Liu [a,b,c,*]

[a] *Jiangsu Co-innovation Center for Prevention and Control of Important Animal Infectious Diseases and Zoonoses, College of Veterinary Medicine, Yangzhou University, Yangzhou 225009, China*
[b] *Joint International Research Laboratory of Agriculture and Agri-Product Safety of MOE, Yangzhou University, Yangzhou 225009, China*
[c] *Institute of Comparative Medicine, Yangzhou University, Yangzhou 225009, China*

ARTICLE INFO

Article history:
Received 24 April 2025
Revised 7 December 2025
Accepted 5 January 2026

Keywords:
Antibiotic adjuvant
5-Fluorouracil
Fosfomycin
MRSA
Pyrimidine metabolism

ABSTRACT

Methicillin-resistant *Staphylococcus aureus* (MRSA) represents a significant global public health threat. Combination therapy, particularly the use of antibiotics in conjunction with non-antibiotic agents, has emerged as a promising strategy to address the growing crisis of antibiotic resistance. Fosfomycin (FOS), increasingly utilized in clinical practice for treating drug-resistant bacterial infections, exhibits limited efficacy as a monotherapy. Here, we find that 5-fluorouracil (5-FU), a Food and Drug Administration (FDA)-approved anticancer drug, effectively enhances the antibacterial activity of FOS against MRSA, including biofilm-embedded MRSA cells. Mechanistically, 5-FU targets cytidine triphosphate (CTP) synthase, a rate-limiting enzyme responsible for the adenosine triphosphate (ATP)-dependent conversion of uridine triphosphate (UTP) to CTP. Moreover, we demonstrate that the synergistic effect of 5-FU and FOS arises from the perturbation of pyrimidine metabolism, which induces membrane damage, dissipation of the proton motive force (PMF), enhanced ATP synthesis, and accumulation of reactive oxygen species, culminating in bacterial death. In both *Galleria mellonella* (*G. mellonella*) and murine infection models, the combination of 5-FU and FOS markedly improves survival and reduces bacterial burdens. Collectively, our work demonstrates the therapeutic potential of 5-FU combined with FOS for tackling MRSA infections and highlights the pivotal role of perturbing pyrimidine metabolism in restoring antibiotic susceptibility.

1. Introduction

Staphylococcus aureus (*S. aureus*), a Gram-positive pathogen, is a major cause of hospital and community-acquired infections, leading to serious consequences. Alarmingly, this bacterium has developed resistance to multiple antibiotic classes [1,2]. A notable example is methicillin-resistant *S. aureus* (MRSA), which was first identified clinically in the early 1960s. The rapid global spread of MRSA strains poses a formidable threat to public health and safety. Currently, MRSA is a leading cause of life-threatening and sometimes fatal infections [3,4]. Traditional treatments for MRSA are highly dependent on antimicrobial agents, but the widespread use of antibiotics has driven MRSA to evolve multidrug resistance [5]. Clinical MRSA infections spread rapidly, exhibit complex resistance mechanisms, and are associated with high mortality rates. In the European Union, nearly 150 000 MRSA infections are reported annually, leading to more than 7 000 deaths [6]. In China, the MRSA infection rate has remained above 30% for the past five years, according to the China Antimicrobial Surveillance Network (CHINET) surveillance system [7].

Despite considerable efforts in developing new antimicrobial drugs, the approval of new antibiotics has been limited in recent decades, creating an urgent need for new anti-infective strategies. Drug combinations, particularly those involving antibiotics and adjuvants, offer a promising and cost-effective approach to circumvent the stagnation in drug discovery and resensitize antibiotic-resistant bacteria [8–10]. For example, a recent study systematically analyzed drug combinations against three Gram-positive bacterial species, revealing the synergistic activity between

* Corresponding author at: Jiangsu Co-innovation Center for Prevention and Control of Important Animal Infectious Diseases and Zoonoses, College of Veterinary Medicine, Yangzhou University, Yangzhou 225009, China.
E-mail address: liuyuan2018@yzu.edu.cn (Y. Liu).

https://doi.org/10.1016/j.eng.2026.01.025

Please cite this article as: J. Luo, Q. Lv, M. He et al., Boosting Fosfomycin Efficacy Against Methicillin-Resistant *Staphylococcus aureus* Infections by Targeting Pyrimidine Metabolism, Engineering, https://doi.org/10.1016/j.eng.2026.01.025

anti-aggregant ticagrelor and cationic antibiotics against *S. aureus* [11]. The combination of antibiotics and adjuvants not only enhances the efficacy of antibiotics but also extends the lifespan of existing antibiotics, delaying the emergence of resistant strains [12]. Moreover, these synergistic therapies can reduce antibiotic toxicity, treatment duration, and dosage requirements [13]. In the current era of resistance, older antibiotics such as polymyxins and fosfomycin (FOS) have regained attention. Discovered over 40 years ago, FOS is a potent bactericidal agent effective against both Gram-negative and Gram-positive bacteria, including multidrug-resistant (MDR) strains. Owing to its unique chemical structure and mechanism of action, FOS inhibits peptidoglycan synthesis at a stage prior to β-lactams, minimizing the likelihood of cross-resistance with other antimicrobial agents [14–16]. As a result, FOS has emerged as a promising candidate for treating systemic infections. However, despite its increasing clinical use, FOS is seldom employed in combination therapies, an approach that warrants further investigation to fully exploit its therapeutic potential.

5-Fluorouracil (5-FU), a Food and Drug Administration (FDA)-approved anticancer agent, primarily functions by inhibiting the synthesis of thymidine monophosphate (dTMP), a nucleotide essential for DNA replication [17,18]. Additionally, central venous catheters coated with 5-FU offer a safe and effective alternative to those coated with chlorhexidine and silver sulfadiazine, particularly for critically ill patients [19]. Previous research has highlighted the potential antibacterial effect of 5-FU against pathogens such as *Escherichia coli* (*E. coli*) and *Streptococcus suis* (*S. suis*) [20]. Additionally, it has been shown to inhibit biofilm formation in *E. coli* while reducing bacterial virulence [21–24]. A recent study demonstrated that 5-FU reversed the resistance of carbapenem-resistant Gram-negative pathogens to meropenem [25]. However, the potential of 5-FU to enhance FOS's efficacy against MRSA has yet to be explored.

In this study, we revealed the capability of 5-FU in effectively potentiating FOS activity against MRSA both *in vitro* and *in vivo*. Combining single nucleotide polymorphism (SNP) analysis of resistant mutants and gene knockout experiments, we identified the cytidine triphosphate (CTP) synthase as the key target of 5-FU. Furthermore, transcriptomic analysis provided insight into the mechanism underlying the synergistic effect of 5-FU and FOS. The perturbation of pyrimidine metabolism was central to their synergy, leading to membrane damage, dissipation of proton motive force (PMF), enhanced adenosine triphosphate (ATP) synthesis, and increased oxidative damage, which ultimately results in bacterial cell death. Our findings highlight the therapeutic potential of combining 5-FU with FOS for treating MRSA-associated infections.

2. Materials and methods

2.1. Bacterial strains and chemical reagents

Table S1 (Appendix A) lists all the strains used in this study. A deletion mutant of *S. aureus* RN4220 was generated using clustered regularly interspaced short palindromic repeats (CRISPR)/CRISPR-associated protein 9 (Cas9)-mediated genome editing tool (pCasSA) and verified by polymerase chain reaction (PCR). Unless otherwise specified, bacterial strains were cultured at 37 °C in Mueller–Hinton broth (MHB) or on Mueller–Hinton agar plates (MHA). Antibiotics used in this study were purchased from Shanghai yuanye Bio-Technology Co., Ltd. (China).

2.2. Broth microdilution assay

The minimal inhibit concentration (MIC) of antibiotics and non-antibiotics was determined according to the Clinical and Laboratory Standards Institute (CLSI) 2021 guidelines using the standard broth microdilution method. Briefly, bacteria grown to the exponential phase were diluted 1:1000 in MHB, and equal volumes of bacterial suspension (1.5×10^6 colony forming units (CFU)·mL^{-1}) were mixed with varying concentrations of antibiotics and non-antibiotics in a sterile 96-well microtiter plate. After incubation at 37 °C for 16 to 18 h, the MIC was defined as the lowest concentration of the antibiotics and non-antibiotics that showed no visible bacterial growth [26].

2.3. Checkerboard analysis

Synergism between FOS and antibiotics or non-antibiotics was assessed using a checkerboard assay with two-fold serial dilutions of the drugs (8 × 8 matrix) [27]. After incubation with a bacterial suspension (1.5×10^6 CFU·mL^{-1}) for 18 h, the absorbance at 600 nm was measured using a microplate reader. The fractional inhibitory concentration index (FICI) was calculated from two biological replicates for each combination using the formula: FICI = (MIC of drug A in combination)/(MIC of drug A alone) + (MIC of drug B in combination)/(MIC of drug B alone). A FICI of ≤ 0.5 indicates synergy.

2.4. Time-dependent killing curve

The overnight culture of MRSA T144 was diluted 1:1000 into fresh MHB and incubated at 37 °C with continuous shaking (200 r·min^{-1}) for 4 h. Cultures were then treated with FOS, 5-FU, or their combination for 24 h. Bacterial counts at 0, 4, 8, and 24 h were determined using the plate colony counting method. MRSA T144 was treated with FOS at 1 μg·mL^{-1} and 5-FU at 16 μg·mL^{-1}, with MHB containing phosphate buffer saline (PBS) as a negative control. Each experiment was repeated three times.

2.5. Flow cytometry analysis

Bacterial viability was analyzed using flow cytometry as previously described [28]. Briefly, exponential-phase bacteria (10^6-CFU·mL^{-1}) were treated with FOS, 5-FU, or their combination at 37 °C and 220 r·min^{-1} for 6 h. Bacterial suspensions were then stained for 15 min with the LIVE/DEAD™ BacLight™ Bacterial Viability Kit (Thermo Fisher Scientific, USA) containing propidium iodide (PI) (5 mmol·L^{-1}, 3 μL) and SYTO 9 (0.835 mmol·mL^{-1}, 3 μL), according to the manufacturer's instructions. After two washes with sterile saline, samples were analyzed using a Flow cytometer (Beckman, USA) with FITC and PI channels. Data were analyzed using CytExpert 2.0 software (Beckman).

2.6. Confocal laser scanning microscopy (CLSM)

MRSA T144 was exposed to FOS (1 μg·mL^{-1}), 5-FU (16 μg·mL^{-1}), or their combination and imaged using CLSM. Bacterial cultures were inoculated into sterile 6-well plates containing the respective drugs, with sterile cell slides placed in the medium. The cultures were incubated for 24 h at 37 °C. After rinsing three times with PBS, the bacteria were stained with SYTO9 and PI. Following a 15 min incubation in the dark, the stained slides were examined using a Leica TCS SP2 CLSM microscope (Heidelberg, Germany).

2.7. Scanning electron microscopy (SEM)

SEM was employed to observe morphological changes in bacteria treated with FOS (1 μg·mL^{-1}), 5-FU (16 μg·mL^{-1}), or their combination, as described previously [29]. Briefly, exponential-phase bacterial cultures (10^6 CFU·mL^{-1}) were incubated with the drugs for 8 h at 37 °C. The bacterial suspensions were centrifuged

(5000*g*, 5 min) and gently washed twice with PBS. The bacterial pellets were then fixed with 2.5% glutaraldehyde (Solarbio, China) for 24 h at 4 °C. After fixation, the bacteria were dehydrated through a series of ethanol gradients (40%, 50%, 60%, 70%, 80%, 90%, and 100%; 10 min each). After gold sputtering, bacterial morphology was examined using a GeminiSEM 300 (ZEISS, Germany).

2.8. Transmission electron microscopy (TEM)

TEM was used to examine the ultrastructural changes in bacteria treated with FOS (1 $\mu g \cdot mL^{-1}$), 5-FU (16 $\mu g \cdot mL^{-1}$), or their combination following previously described methods [30]. Briefly, bacterial suspensions were centrifuged and resuspended in 1 mL of fixative solution containing 2.5% glutaraldehyde and 5% formaldehyde. Fixed bacteria were washed three times with 0.1 $mol \cdot L^{-1}$ cacodylate buffer and post-fixed with 1% osmium tetroxide for 1 h. After three washes with water, bacteria were further dehydrated using ethanol gradients (10 min each: 50%, 60%, 70%, 80%, 90%, and 100%). Samples were infiltrated with Epon™ (Sigma, USA) resin and polymerized at 75 °C for 48 h. Ultrathin sections were cut with a diamond knife, picked up on copper grids, and stained with lead citrate. Cell micrographs were obtained using a JEM 1011 TEM (JEOL, Japan).

2.9. Biofilm inhibition assay

The inhibitory effect of 5-FU and FOS on biofilm formation was evaluated according to a previously described protocol [31]. Specifically, 24 mm diameter cell slides were placed at the bottom of each well in a 6-well plate (Corning, USA). 2 mL of bacterial culture treated with FOS, 5-FU, or their combination was added to each well. After 24 h of incubation at 37 °C, planktonic bacteria were removed, and biofilms were stained with 1% crystal violet (Solarbio) for 15 min. The slides were washed three times with distilled water, and biofilms were solubilized with 33% acetic acid. The absorbance at 570 nm was measured using a microtiter plate reader to quantify biofilm formation.

2.10. Treatment of pre-formed biofilms

Mid-exponential phase cultures were diluted to 10^6 $CFU \cdot mL^{-1}$ in MHB medium. In a 6-well plate, 2 mL of the bacterial suspension was added to each well, and the plates were incubated for 36 h at 37 °C to form mature biofilms [32]. After removing the planktonic bacteria, 2 mL of MHB containing FOS, 5-FU, or their combination was added to the remaining biofilm cells, and the plates were incubated for an additional 24 h at 37 °C. Following incubation, the plates were sonicated at 50 W for 10 min to detach the adhered bacteria, and the number of viable bacteria was determined by microbiological counting.

2.11. Resistance development and single nucleotide polymorphism (SNP) analysis

The ability of 5-FU to induce resistance in MRSA T144 was studied as described previously [33]. The intermediate and final MICs were monitored after 20 consecutive passages in the presence of the test drug (0.5-fold MIC), and the fold-change increase in MIC was recorded. During the induction process, bacterial cultures were stored at −80 °C in 20% glycerol. Genomic DNA from the MIC mutant strains was extracted, and whole-genome fragment libraries were prepared using the paired-end Sample Preparation Kit (Illumina, USA). The genomes were sequenced on an Illumina HiSeq 2500 platform (Illumina) and assembled using *de novo* SPAdes Genome Assembler (version 3.12.0) [33]. The resulting reads were mapped to the MRSA T144 reference genome, and mutations were identified using Snippy.

2.12. Molecular docking analysis

The receptor protein structure was downloaded from the Protein Data Bank (PDB) and UniPort (NDK:PDB ID: 3Q83; CTP synthase: UniPort ID: Q2FF01), along with the chemical structure of 5-FU (PubChem CID: 3385). These were converted into mol2 format for molecular docking. Ligand molecules and the receptor protein were pre-processed using PyMOL software. AutoDock Vina, a docking tool within AutoDock Tools, was used to perform the docking analysis. The model with the lowest binding energy was selected for interaction analysis, and two-dimensional (2D) and three-dimensional (3D) structure models were generated using Discovery Studio 4.5 [34].

2.13. Gene knockout

Gene knockout experiments were conducted in *S. aureus* RN4220 according to a previously described protocol [35]. Primers used for PCR are listed in Table S2 in Appendix A, and were synthesized by Youkang Biotech (China). Changes in the MIC for 5-FU and FOS in the knockout strain were measured, and the impact of thymine supplementation on bacterial growth and drug combination efficacy was also assessed.

2.14. Transcriptome sequencing

The transcriptome of MRSA T144 after treatment with FOS (1 $\mu g \cdot mL^{-1}$), 5-FU (16 $\mu g \cdot mL^{-1}$), or their combination were analyzed in log-phase bacteria. Briefly, MRSA cultures were treated with different treatments for 8 h. Afterwards, the bacterial suspension was centrifuged (5000*g*, 5 min), and the total RNA was extracted and quantified using a Nanodrop spectrophotometer (Thermo Scientific, USA). Sequencing was performed using the Illumina Hiseq 2000 system (Majorbio, China). Differential gene expression was analyzed using the edgeR software. Genes with a false discovery rate (FDR) < 0.05 and $|\log_2 \text{fold change}| \geq 1$ were considered significantly differentially expressed [36].

2.15. Untargeted metabolomics analyses

Metabolites extracted from MRSA T144 with or without 5-FU treatment were analyzed using a UPLC-Q-Exactive Orbitrap mass spectrometer (Thermo Fisher Scientific). Samples were subjected to liquid chromatography (LC) for component separation, followed by ionization in the high-vacuum mass spectrometer. The separated ions were analyzed based on their mass to charge ratio (m/z), generating mass spectra (50–750 m/z). The mass spectrometric data were analyzed to obtain both qualitative and quantitative results. Each sample was analyzed in both positive and negative ionization modes. Metabolites were characterized by comparing retention times, mass ratios, and fragmentation patterns. Internal standards were used to ensure consistency between chromatography and injection.

2.16. Reverse Transcription Quantitative polymerase chain reaction (RT-qPCR) anlaysis

Total RNA was extracted from MRSA T144 using the RNeasy Mini Kit (Vazyme, China) according to the manufacturer's instructions. A total of 500 ng of purified RNA was reverse transcribed into complementary DNA (cDNA) using the RT Master Kit (Takara, Japan). The PCR reaction mixture was prepared using TB Green Premix Ex Taq™ (Vazyme). Amplification conditions were as follows:

initial denaturation at 95 °C for 30 s, followed by 40 cycles of 95 °C for 5 s, 60 °C for 30 s, and 72 °C for 45 s. The 16S ribosomal RNA (rRNA) expression level was used as an internal control, and changes in other gene expressions were analyzed using the comparative cycle threshold (CT) method [37]. Primers used are listed in Table S2, and were synthesized by Youkang Biotech.

2.17. Cytoplasmic membrane potential

Membrane potential changes after treatment with FOS (1 μg·mL^{-1}), 5-FU (16 μg·mL^{-1}), or their combination were assessed using 3,3′-dipropylthiadicarbocyanine iodide ($DiSC_3(5)$, 0.5 μmol·L^{-1}) [38]. Bacterial samples were incubated with $DiSC_3(5)$ for 30 min, followed by treatment with FOS, 5-FU or their combination for 1 h. Membrane potential dissipation was measured using an excitation wavelength of 622 nm and an emission wavelength of 670 nm.

2.18. Cell membrane permeability

Cell membrane permeability was evaluated using PI [39]. Briefly, bacterial suspensions were incubated with PI (final concentration, 5 μmol·L^{-1}) for 30 min, followed by treatment with FOS, 5-FU, or their combination for 1 h. Membrane permeability was measured using an Infinite E Plex microplate reader (Tecan, Switzerland) at excitation/emission wavelengths of 535 nm/615 nm.

2.19. Evaluation of protein leakage

The Enhanced BCA Protein Assay Kit (Beyotime, China) [40] was used to detect protein leakage. Briefly, MRSA T144 was washed twice with PBS (pH = 7.4) using a refrigerated centrifuge (6000 r·min^{-1}) for 5 min and diluted in PBS to the desired working concentration at an OD_{600} of 0.5. After treatment with FOS, 5-FU, or their combination for 4 h, the bacterial suspension was centrifuged (6000 r·min^{-1}) for 5 min. The supernatant was immediately collected and the relative protein leakage of each sample was determined using a microplate reader at OD_{562}.

2.20. ΔpH measurement

Exponentially growing bacterial suspensions were centrifuged, washed with PBS, and incubated with the pH-sensitive fluorescent probe 2′,7′-bis-(2-carboxyethyl)-5-(and-6)-carboxyfluorescein, acetoxymethyl ester (BCECF-AM) (1 μmol·L^{-1}) [41] at 37 °C in the dark for 30 min. The samples were then treated with FOS (1 μg·mL^{-1}), 5-FU (8 μg·mL^{-1}), or their combination at 37 °C for 1 h. Fluorescence at 488 nm excitation and 535 nm emission wavelengths was measured to calculate pH changes.

2.21. L-Lactate measurement

L-Lactate concentration in bacteria treated with FOS, 5-FU, or their combination was measured using the L-Lactate Assay Kit with WST-8 (Beyotime). Briefly, MRSA T144 were cultured at OD_{600} at an 0.5, and after treatment with FOS, 5-FU, or their combination for 4 h, the bacterial suspension was centrifuged (6000 r·min^{-1}) for 5 min. The supernatants were then collected for measurement following the instructions.

2.22. Reactive oxygen species (ROS) measurement

ROS levels in MRSA T144 treated with FOS, 5-FU, or their combination were measured using 2′,7′-dichlorodihydrofluorescein diacetate (DCFH-DA, 10 μmol·L^{-1}) [42]. The bacterial samples were incubated with DCFH-DA at 37 °C for 30 min, washed twice with PBS to reduce extracellular fluorescence, and treated with FOS, 5-FU, or their combination for 1 h. Fluorescence intensity (λexcitation/λemission, 488/525 nm) was measured using a microplate reader (Tecan, Switzerland).

2.23. Intracellular ATP measurement

Intracellular ATP levels in MRSA T144 were measured using an enhanced ATP detection kit (Beyotime) [43]. Exponentially growing bacteria were incubated with FOS (1 μg·mL^{-1}), 5-FU (16 μg·mL^{-1}), or their combination for 1 h. Bacterial pellets were collected by centrifugation, and lysed to release ATP. The intracellular ATP levels were quantified using luminescence signals on a microplate reader.

2.24. Measurement of 8-hydroxy-2′-deoxyguanosine (8-OHdG) and dihydroorotate dehydrogenase (DHODH) levels

The levels of 8-OHdG and DHODH in MRSA T144 treated with 5-FU, FOS, or their combination were measured using an 8-OHdG ELISA kit (Sangon Biotech, China) and a DHODH kit (Mlbio, China), respectively [44]. Bacterial cultures in the exponential phase were treated with 5-FU and FOS, and the supernatants were collected for measurement following the kit instructions.

2.25. Nicotinamide adenine dinucleotide (NAD^+)/nicotinamide adenine dinucleotide (NADH) determination

The MRSA T144 strain was cultured to the exponential phase, treated with 5-FU and FOS, and the bacterial cultures were collected, centrifuged, and resuspended. The NAD^+/NADH ratio was determined using an NAD^+/NADH Assay Kit (Beyotime), following the manufacturer's instructions.

2.26. Ethics approval

This study was conducted in accordance with the ethical guidelines set by the Jiangsu Laboratory Animal Welfare and Ethics Committee of the Jiangsu Administrative Committee of Laboratory Animals (SYXK-2022-0044). All animal experiments were approved by the Animal Care Committee of Yangzhou University.

2.27. Galleria mellonella (G. mellonella) infection model

G. mellonella (Huide BioTech, China) larvae were randomly divided into four groups (n = 8 per group) and infected with 10 μL of MRSA T144 suspension (1.0×10^6 CFU) injected into the right proleg [26,41]. One hour after infection, larvae were treated in the left proleg with PBS, FOS alone (10 mg·kg^{-1}), 5-FU alone (40 mg·kg^{-1}), or their combination. Survival was monitored over 120 h.

2.28. Mouse peritonitis infection model

Female ICR mice (n = 6 per group) were intraperitoneally infected with a lethal dose of 1.0×10^8 CFU MRSA T144 suspension. One hour after infection, mice were administered FOS (10 mg·kg^{-1}), 5-FU (40 mg·kg^{-1}), or their combination by intraperitoneal injection. Mouse survival was tracked for 7 d, and bacterial loads in homogenates of the heart, liver, spleen, lungs, and kidneys were determined by colony counting following serial dilution and incubation at 37 °C for 18 h.

2.29. Statistical analyses

Statistical analyses were performed using GraphPad Prism 9.5.0 (Software Inc., USA). Data are presented as the mean ± standard deviation (SD). Statistical significance was determined using an

unpaired two-tailed Student's *t*-test for comparisons between two groups, or by one-way ANOVA with Dunnett's or Tukey's *post-hoc* test for comparisons among more than two groups. Differences between groups were considered significant at $P < 0.05$ ($^{*}P < 0.05$, $^{**}P < 0.01$, $^{***}P < 0.001$, $^{****}P < 0.0001$).

3. Results

3.1. Synergistic activity of 5-FU and FOS against MRSA strains

To identify the compounds that can potentiate the activity of FOS against MDR Gram-positive bacteria, we tested the synergistic activity of FOS and 30 antibiotics or non-antibiotics against *Enterococcus faecium* (*E. faecium*) A4 (VRE, VanA), *S. aureus* G16 (RIF^R), and MRSA 1530, respectively. These clinical strains displayed an MDR phenotype (Table S2). As shown in Fig. S1 in Appendix A, checkerboard assays revealed that FOS exhibited synergistic activity with several compounds, including linezolid, moxifloxacin, and 5-FU, against MRSA. Notably, 5-FU displayed a potent synergistic effect with FOS against both *S. aureus* G16 and MRSA 1530, with the FICI values of 0.3125 and 0.375, respectively (Fig. 1(a)). No synergistic effect was observed in *E. faecium* A4, suggesting species-specific action. Moreover, the potentiation of 5-FU to FOS was also found in another clinically relevant MRSA strain, T144 (FICI, 0.375) (Fig. 1(b)). We next performed time-killing curves to evaluate the bactericidal dynamics of 5-FU and FOS, either alone or in combination, against MRSA T144. The results showed minimal impact on MRSA T144 growth with either monotherapy. However, after 8 h of combined treatment, bacterial loads were significantly reduced, with a 3–6 $\log_{10}$ decrease compared to monotherapy or untreated control (Fig. 1(c)). Additionally, bacterial viability was assessed via flow cytometry using PI and SYTO 9 co-staining. Consistently, the combination treatment reduced bacterial viability to approximately 65%, while control and FOS alone sustained approximately 98% survival, and 5-FU alone modestly reduced viability to approximately 80% (Figs. 1(d) and (e)). These results indicated that 5-FU has limited antibacterial activity, whereas its combination with FOS induces pronounced bacterial lethality. Meanwhile, we monitored the live/dead state of MRSA cells under different treatments using confocal laser scanning microscope (CLSM). Compared to FOS monotreatment, the combination treatment resulted in decreased green fluorescence and increased red fluorescence, indicating increased cell death (Fig. 1(f)). SEM of the control and monotreatment group showed regular and intact cell surfaces (Fig. 1(g)). In contrast, cells treated with the combination of FOS and 5-FU displayed severe cellular damage, including irregular and collapsed surfaces. These results were further confirmed through TEM, which demonstrated that control and monotreatment cells maintained a smooth, circular morphology and intact cell walls, while cells treated with the combination exhibited compromised bacterial cell wall and membrane integrity (Fig. 1(g)).

Biofilm formation is a critical virulence factor in MRSA infections, providing protection against antimicrobial treatments. To assess the anti-biofilm ability of the FOS (1 $\mu g \cdot mL^{-1}$), 5-FU (16 $\mu g \cdot mL^{-1}$) and their combination, we performed CLSM and crystal violet staining. As shown in Fig. S2(a) in Appendix A, the combination of FOS and 5-FU significantly reduced biofilm formation. Additionally, we evaluated the efficacy of this combination against mature biofilms. The results indicated a substantial reduction in biofilm cell loads following combination treatment (Fig. S2(b) in Appendix A). These results demonstrate the excellent synergistic activity of 5-FU and FOS against MRSA, including biofilm-embedded cells.

3.2. 5-FU targets bacterial CTP synthase

To investigate the mechanisms underlying the action of 5-FU, we performed RNA sequencing on MRSA cells with or without 5-FU treatment. Kyoto Encyclopedia of Genes and Genomes (KEGG) enrichment analysis revealed that the upregulated differentially expressed genes (DEGs) were primarily associated with pathways related to the ribosome, homologous recombination, mismatch repair, DNA replication, RNA polymerase, and pyrimidine metabolism. In contrast, the downregulated DEGs were linked to *S. aureus* infection, cationic antimicrobial peptide (CAMP) resistance, two-component systems, fatty acid degradation, teichoic acid biosynthesis, and sulfur metabolism (Figs. 2(a) and (b)). These results suggested that 5-FU has potential therapeutic applications in managing *S. aureus*-associated infections, with its action likely involving the inhibition of DNA synthesis, particularly through pathways related to pyrimidine metabolism.

To further explore the potential targets of 5-FU, MRSA T144 was continuously exposed to sub-MICs of 5-FU for 15 d. Consequently, the MIC values of 5-FU increased from 64 to 512 $\mu g \cdot mL^{-1}$ (an eight-fold increase) (Fig. 2(c)). However, long-term co-treatment with 5-FU and FOS effectively prevented the development of resistance to either agent, as shown in Fig. S3 in Appendix A. Whole-genome SNP analysis revealed mutations in several genes, including *sdrC* (encoding an adhesin), *erm*(C) (encoding a 23S rRNA methyltransferase), *fnbA/B* (encoding fibronectin-binding proteins), *bin* (encoding a resolvase/integrase), and various metabolic genes such as those involved in deoxyribose-phosphate aldolase and riboflavin biosynthesis enzymes. Based on these findings, we examined the CTP synthase (encoded by the *pyrG* gene), which is involved in both nucleic acid and phospholipid biosynthesis (Fig. 2(d) and Table S3 in Appendix A). To verify this, we knocked out the *pyrG* gene in *S. aureus* and determined the corresponding changes in MIC (Figs. 2(e) and (f)). The Δ*pyrG* displayed a two-fold increase in MIC value to 5-FU compared to the wild-type (WT) strain (Fig. 2(g)). Additionally, we monitored the bacterial growth of WT and Δ*pyrG* in the presence of 5-FU. Consistently, Δ*pyrG* displayed a higher level of resistance to 5-FU (Fig. 2(h)), implying that CTP synthase may be a potential antibacterial target of 5-FU. Furthermore, we assessed the interaction between 5-FU and CTP synthase via molecular docking. The results indicated that 5-FU could bind to the key amino acid residues (e.g., GLU510, HIS508, VAL59, and ARG461) of CTP synthase via Van der waals, hydrogen bond and Pi–Pi T-shaped interactions (Fig. 2(i)).

Considering the important role of CTP synthase in pyrimidine metabolism, we reasoned that 5-FU may inhibit DNA synthesis and induce bacterial death (Fig. S4(a) in Appendix A). To verify this hypothesis, we performed targeted metabolomic analysis of pyrimidine metabolism-related metabolites in MRSA cells with or without 5-FU treatment. Notably, significant enrichment of the pyrimidine metabolism pathway was observed in MRSA T144 cells treated with 5-FU (Figs. S4(b) and (c) in Appendix A). Specifically, a dramatic decrease in thymine levels was found in 5-FU-treated cells (Fig. S4(d) in Appendix A), whereas the addition of exogenous thymine reduced the inhibitory effect of 5-FU against MRSA (Fig. S4(e) in Appendix A). To further confirm the role of CTP synthase inhibition in the antibacterial and synergistic action of 5-FU, we performed rescue assays by adding the medium with cytidine, the direct product of CTP synthase. Consequently, cytidine supplementation led to a two-fold increase in the MIC of 5-FU, while the FOS MIC remained unchanged (Fig. S5(a) in Appendix A). Moreover, checkerboard assays indicated that the FICI increased from 0.375 to 0.5 (Fig. S5(b) in Appendix A), indicating a weakened synergistic effect. These results suggest that inhibiting CTP synthase is a critical, though not exclusive, determinant of 5-FU activity and its synergism with FOS.

3.3. 5-FU and FOS combination results in pyrimidine metabolism perturbation

To gain a deeper understanding of their synergistic mechanisms, we performed transcriptomic analysis of MRSA cells treated with PBS, FOS or a combination with 5-FU (Fig. 3(a)). A total of

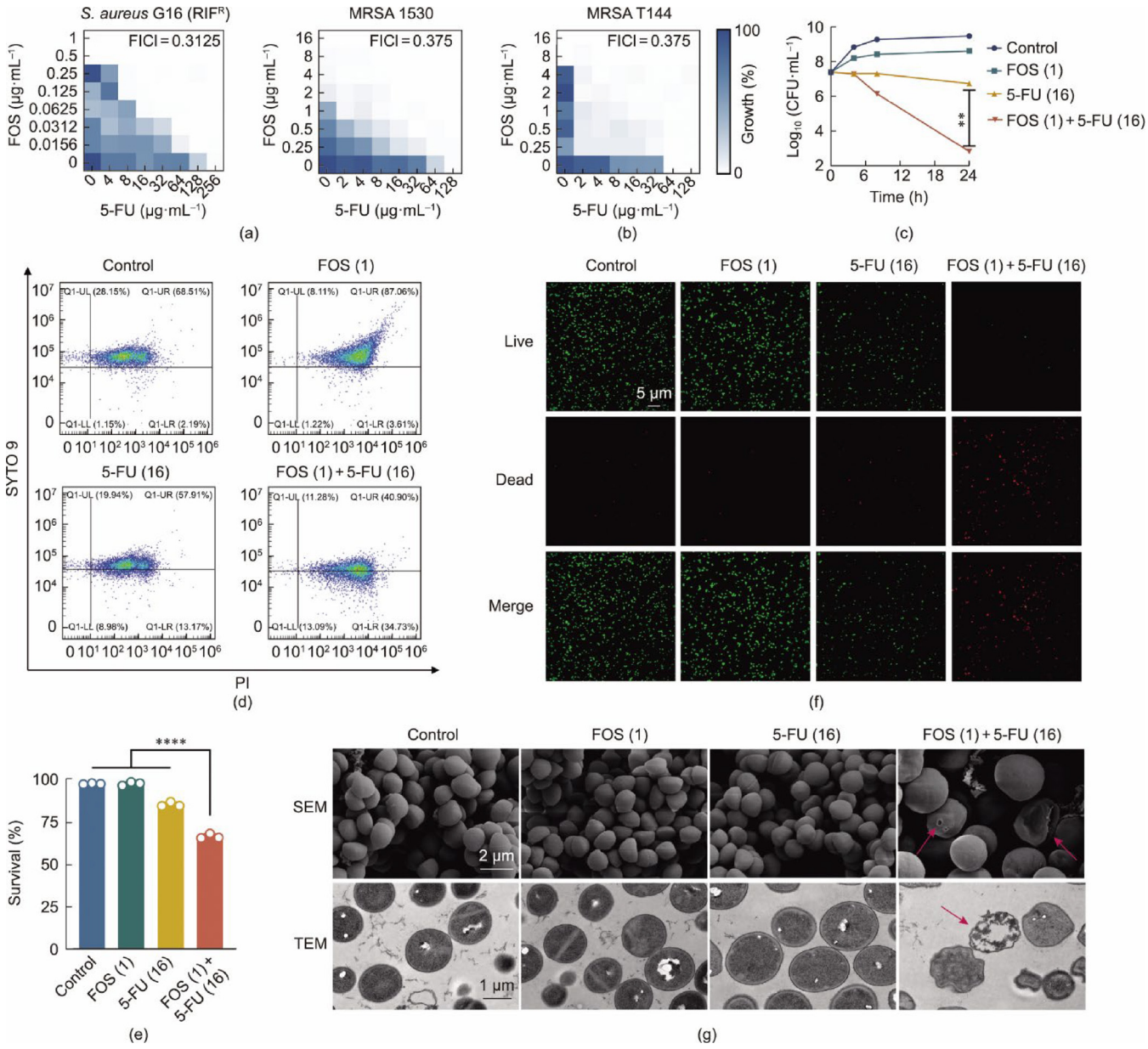

Fig. 1. 5-FU potentiates the antibacterial activity of FOS against MRSA. (a) Checkerboard assay of 5-FU and FOS in inhibiting the growth of *S. aureus* G16 and MRSA 1530. After 18 h of incubation at 37 °C, OD600 was measured, and the FICI values were calculated. Synergy: FICI ≤ 0.5; no interaction: 0.5 < FICI ≤ 4; antagonism: FICI > 4. Experiments were performed in two independent replicates. (b) Synergistic activity of FOS and 5-FU against MRSA T144, with a FICI of 0.375. (c) Time-kill curves of 5-FU and FOS against MRSA T144. (d) Flow cytometry analysis of live/dead bacterial ratios after 6 h treatment with 5-FU and FOS alone or in combination. Live and dead bacteria were stained green and red, respectively. LL: lower left; UL: upper left; LR: lower right; UR: upper right. (e) Bacterial survival rates quantified by flow cytometry. (f) CLSM analysis of MRSA T144 treated with 5-FU and FOS alone or in combination. (g) Microscopic images of MRSA T144 after 24 h of single treatment or in combination observed through SEM/TEM. Data are shown as mean ± SD. *P* value was determined by (c) unpaired *t*-test or (e) one-way analysis of variance (ANOVA). $^{**}P < 0.01$, $^{****}P < 0.0001$.

1425 DEGs were identified by comparing the combination treatment with the PBS group, with 730 up-regulated and 695 down-regulated (Fig. 3(b)). Cluster and KEGG analyses showed that the up-regulated DEGs were predominantly associated with ribosome, mismatch repair and pyrimidine metabolism pathway, while down-regulated DEGs were involved in two-component systems and ATP-binding cassette (ABC) transporters (Fig. 3(c)). The expression patterns of representative genes related to these pathways were depicted in Fig. 3(d). Additionally, up-regulation of the pyrimidine metabolism were also observed in the comparison of the combination and FOS treatment alone (Fig. S6 in Appendix A). Consistently, RT-qPCR analysis confirmed the increased expression of pyrimidine metabolism pathway-related genes under combination treatment (Fig. S7 in Appendix A), particularly for *pyrG* and *ndk* genes (Fig. 3(e)). These results implied that the pyrimidine metabolism was the major affected pathway in MRSA T144 following combination therapy.

To further ascertain the impact of this combination on pyrimidine biosynthesis, which is crucial for bacterial growth and nucleic acid synthesis, we monitored the changes of DHODH, a key enzyme in pyrimidine synthesis that catalyzes the conversion of dihydroorotate (DHO) to orotate (ORO). Loss of DHODH has been shown to impair respiratory chain complex III function, reduce mitochondrial membrane potential, and induce ROS generation [45]. Our measurements showed that DHODH levels in bacteria treated with the 5-FU and FOS combination were significantly

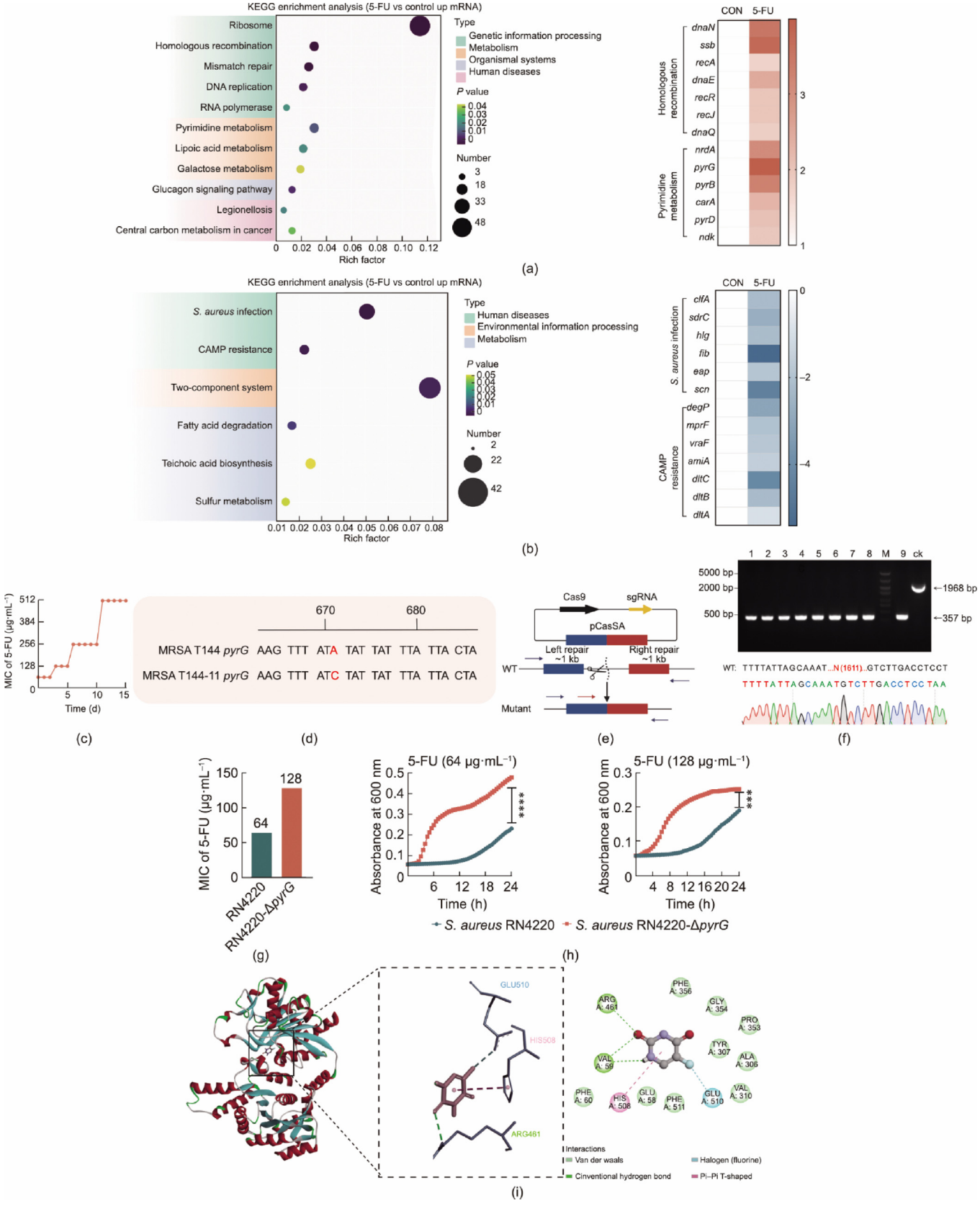

Fig. 2. 5-FU targets bacterial CTP synthase. (a, b) KEGG pathway enrichment analysis comparing the combination versus control group. The ordinate represents the significantly enriched pathways. (c) Development of resistance to 5-FU in MRSA T144. (d) SNP analysis of CTP synthase (*pyrG*). (e) Schematic illustration of the gene knockout procedures. The blue arrows are the primers utilized for PCR validation of the editing efficiency. The red arrow is the primer used for sequencing. (f) pCasSA-mediated deletion of the *pyrG* gene in the *S. aureus* RN4220. The lane labeled "ck" is the PCR product from the WT strain as a control. (g) Changes in the MIC of 5-FU against the mutant strains. (h) Growth curves of *S. aureus* RN4220 and *S. aureus* RN4220-Δ*pyrG* in the presence of 5-FU at 64 or 128 μg·mL^{-1}. (i) Molecular docking analysis of CTP synthase with 5-FU, the 2D diagram depicts interaction modes and binding sites. GLU: glutamate; HIS: histidine; ARG: arginine; PHE: phenylalanine; GLY: glycine; PRO: proline; TYR: tyrosine; ALA: alanine; VAL: valine. Data are shown as mean ± SD. *P* value was determined by unpaired *t*-test in (h, m, n). ***$P < 0.001$, ****$P < 0.0001$.

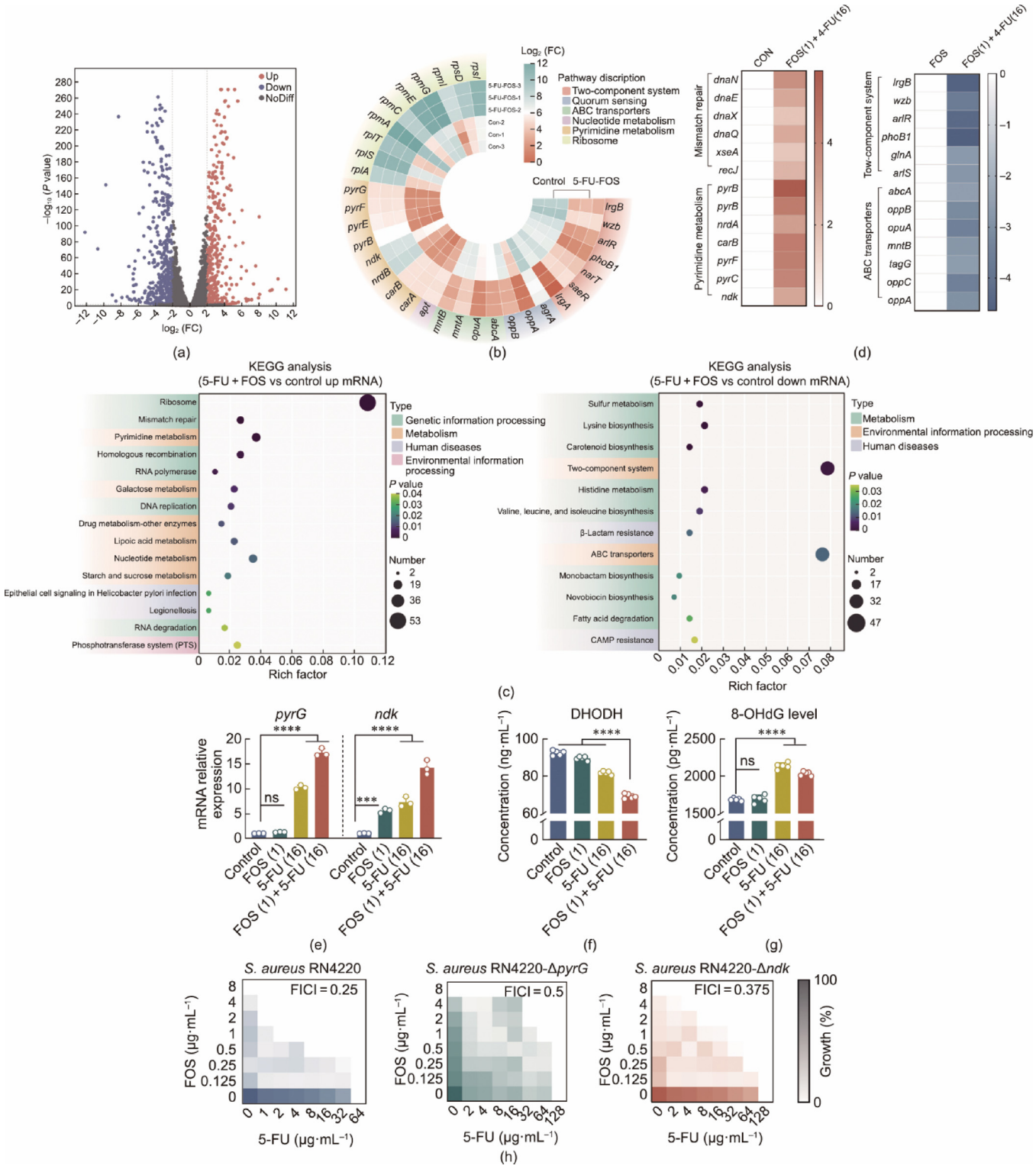

Fig. 3. The combination of 5-FU and FOS perturbs pyrimidine metabolism. (a) Volcano plot visualizing the distribution of DEGs. Downregulated and upregulated genes are denoted by blue and red dots, respectively. NoDiff: no difference. (b) Heatmap of clustering of selected DEGs. (c) KEGG pathway enrichment analysis. The ordinate displays significantly enriched pathways, indicating that pyrimidine metabolism, mismatch repair, two-component systems, and ABC transporter-related pathways were markedly affected. (d) Expression patterns of representative genes associated with the aforementioned KEGG pathways. (e) Differential expression levels of the *ndk* and *pyrG* genes in the monotherapy and combination groups. (f, g) Levels of (f) 8-OHdG and (g) DHODH in MRSA T144 following treatment with 5-FU, FOS, or their combination. (h) Comparison of the synergistic effects of 5-FU combined with FOS against three *S. aureus* (RN4220, RN4220-Δ*pyrG*, and RN4220-Δ*ndk*). Data are shown as mean ± SD. *P* values in (e–g) were determined by one-way ANOVA. ***$P < 0.001$, ****$P < 0.0001$, ns: not significant.

reduced, suggesting that the combination disrupted pyrimidine biosynthesis (Fig. 3(f)). Considering the importance of pyrimidine metabolism in DNA synthesis and repair, we further monitored the effect of 5-FU and FOS combination on bacterial DNA damage by measuring the content of 8-hydroxy-2′-deoxyguanosine (8-OHdG). The results showed that intracellular 8-OHdG levels were

significantly elevated under combination treatment, indicating that the combination induced substantial bacterial DNA damage (Fig. 3(g)). These results demonstrated that the combination of 5-FU and FOS disturbs pyrimidine metabolism, leading to DNA damage in MRSA.

To confirm the role of pyrimidine metabolism perturbation in the synergistic activity of 5-FU and FOS, we knocked out the *ndk* gene, encoding nucleoside diphosphate kinase, which facilitates the reversible transfer of the γ-phosphate from nucleoside triphosphates to nucleoside diphosphates (Fig. S8 in Appendix A). We further tested the synergistic effects of 5-FU and FOS in two mutant strains (Δ*pyrG* and Δ*ndk*). The results showed that the deletion of *ndk* modestly weakened the synergism of this combination, whereas *pyrG* deficiency completely abolished their synergistic activity (Fig. 3(h)), indicating that the targeting effect of 5-FU on CTP synthase is essential for its potentiation to FOS.

Given the critical roles of *pyrG* and *ndk* genes in the pyrimidine metabolism (Fig. 4(a)), we further assessed the effect of exogenous supplementation of pyrimidine metabolites (cytosine, uracil, and thymine) on the synergistic effect of 5-FU and FOS in WT and its mutant strains (Δ*pyrG* and Δ*ndk*). Supplementation with these metabolites reduced the synergy in all three strains, as demonstrated by the checkerboard assay (Figs. 4(b)–(d)). Consistent with this, time-killing assays indicated that supplementation with pyrimidine metabolites weakened or eliminated the synergistic bactericidal effect of 5-FU and FOS (Fig. 4(e)). These results collectively indicate that the synergistic activity between 5-FU and FOS is highly dependent on the perturbation of pyrimidine metabolism pathway.

3.4. Combination of 5-FU and FOS induces membrane dysfunction and oxidative damage

Next, we sought to elucidate how the combination of 5-FU and FOS eventually causes bacterial cell death. First, we assessed the impact of this combination on the membrane permeability of MRSA T144 using PI, a red-fluorescent dye that penetrates only dead or damaged cells. Compared to individual treatments with FOS or 5-FU, the combination resulted in increased fluorescence intensity, indicating increased membrane permeability (Fig. 5(a)). Consistently, protein-leakage assays confirmed that the combination treatment caused markedly more membrane damage than either monotreatment or control groups (Fig. S9 in Appendix A). Bacterial PMF, generated by electron transport chain activities, is essential for bacterial survival [46]. Then, we assessed the impact of this combination on PMF using $DiSC_3(5)$ probe, which accumulates in the cytoplasmic membrane in response to the membrane potential ($\Delta\Psi$) component of PMF. When $\Delta\Psi$ is disrupted, the probe is released into the extracellular environment, causing an increase in fluorescence. As shown in Fig. 5(b), the combination of 5-FU and FOS resulted in increased fluorescence compared with monotreatment, indicating that their combination exacerbated PMF dissipation. Meanwhile, we assessed the effect of their combination on transmembrane proton gradient (ΔpH) using a fluorescent probe BCECF-AM. In agreement with the dissipation of $\Delta\Psi$, the combination treatment led to an increase in ΔpH, reflecting their complementary mechanisms (Fig. 5(c)).

Inspired by the transcriptomic evidence that the combination treatment interfered with energy metabolism, we next examined key indicators of bacterial energetics. The results showed that the ratio of NAD^+/NADH was reduced under the combination treatment (Fig. 5(d)). Meanwhile, this combination led to an increase of intracellular ATP levels in MRSA T144 (Fig. 5(e)). The dissipation of PMF appears to contradict the observed increase in ATP production under combination treatment. To further investigate this, we conducted transcriptomic and RT-qPCR analyses, revealing upregulation of oxidative phosphorylation genes (e.g., *atpA/C/D/F/G*) and fatty acid biosynthesis genes (*accA/B/C*) (Figs. S10(a) and (b) in Appendix A). This suggests a compensatory mechanism to enhance respiratory activity and restore membrane integrity. Moreover, elevated *L*-lactate levels (Fig. S10(c) in Appendix A) indicated increased substrate-level phosphorylation, which likely serves as a rapid energy-generating alternative pathway. To confirm the role of glycolysis, we measured ATP levels in the presence of the glycolysis inhibitor 2-deoxy-*D*-glucose (2-DG). A significant reduction in ATP levels upon 2-DG addition (Fig. S10(d) in Appendix A) indicated that glycolysis becomes the predominant ATP-generating pathway in response to the 5-FU and FOS combination (Fig. S10(e) in Appendix A). These findings align with a recent study that suggested antibacterial efficacy is often linked to excessive bacterial ATP production [47].

Imbalances in the NAD^+/NADH ratio are known to trigger ROS production [48,49]. Using the fluorescent probe DCFH-DA, we found that the combination of 5-FU and FOS significantly elevated intracellular ROS levels (Fig. 5(f)). In contrast, the addition of ROS scavenger *N*-acetylcysteine (NAC) [50] effectively mitigated the ROS elevation induced by 5-FU treatment in a dose-dependent manner (Fig. 5(f)) and abolished the synergistic activity of the combination (Figs. 5(g) and (h)). Notably, a high concentration of NAC (10 $mmol \cdot L^{-1}$) increased the MICs of both FOS and 5-FU by two-fold (Fig. S11(a) in Appendix A). In contrast, NAC had no effect on the synergism between FOS and linezolid/moxifloxacin (Fig. S11(c) in Appendix A). These findings indicated that ROS generation was crucial for the synergistic activity between 5-FU and FOS. To explore the link between CTP synthase inhibition and ROS production, we measured ROS levels in the Δ*pyrG* strain. Strikingly, compared to the WT strain, the deletion of *pyrG* resulted in a significant increase in ROS generation (Fig. S12 in Appendix A), indicating that 5-FU-mediated CTP synthase inhibition exacerbates oxidative damage in bacteria. Conversely, the addition of NAC significantly reduced ROS levels in the Δ*pyrG* strain, underscoring the role of pyrimidine metabolism in modulating ROS accumulation. These mechanistic studies demonstrate that the combination of 5-FU and FOS disturbs bacterial pyrimidine metabolism, which further causes membrane damage, increased ATP synthesis and ROS generation, ultimately resulting in bacterial death (Fig. 6).

3.5. In vivo efficacy evaluation of 5-FU and FOS

Given the potent *in vitro* synergy of 5-FU and FOS against MRSA, we assessed the *in vivo* efficacy in two animal infection models (Fig. 7(a)). Prior to this, we assessed the safety of 5-FU to ensure that the administered dose would not induce potential toxic effects. A dose of 40 $mg \cdot kg^{-1}$ of 5-FU was administered to both *G. mellonella* and mice (Fig. S13(a) in Appendix A). Over the 7-d observation period, all individuals in the PBS control and 5-FU treatment groups survived (Fig. S13(b) in Appendix A). Additionally, mice treated with 5-FU exhibited normal weight gain (Fig. S13(c) in Appendix A). To further assess potential toxicity, we analyzed serum biochemical parameters and histological sections of the liver and kidney (hematoxylin and eosin (H&E) staining) after 7 d of treatment (Figs. S13(d) and (e)). No significant differences were observed between the PBS and 5-FU groups, indicating that 40 $mg \cdot kg^{-1}$ of 5-FU does not induce detectable toxicity in eukaryotic hosts. These results confirm that the *in vivo* infection models are not confounded by host toxicity from 5-FU.

Next, we evaluated the effectiveness of the combination of 5-FU and FOS in *G. mellonella* and murine infection models. In the *G. mellonella* infection model, larvae infected with MRSA T144 treated with PBS all died within 48 h, and the survival rate of *G. mellonella* treated with monotherapy was only 37.5% after 5 d. In contrast, the survival rate in the combination treatment group reached 100% (*P*

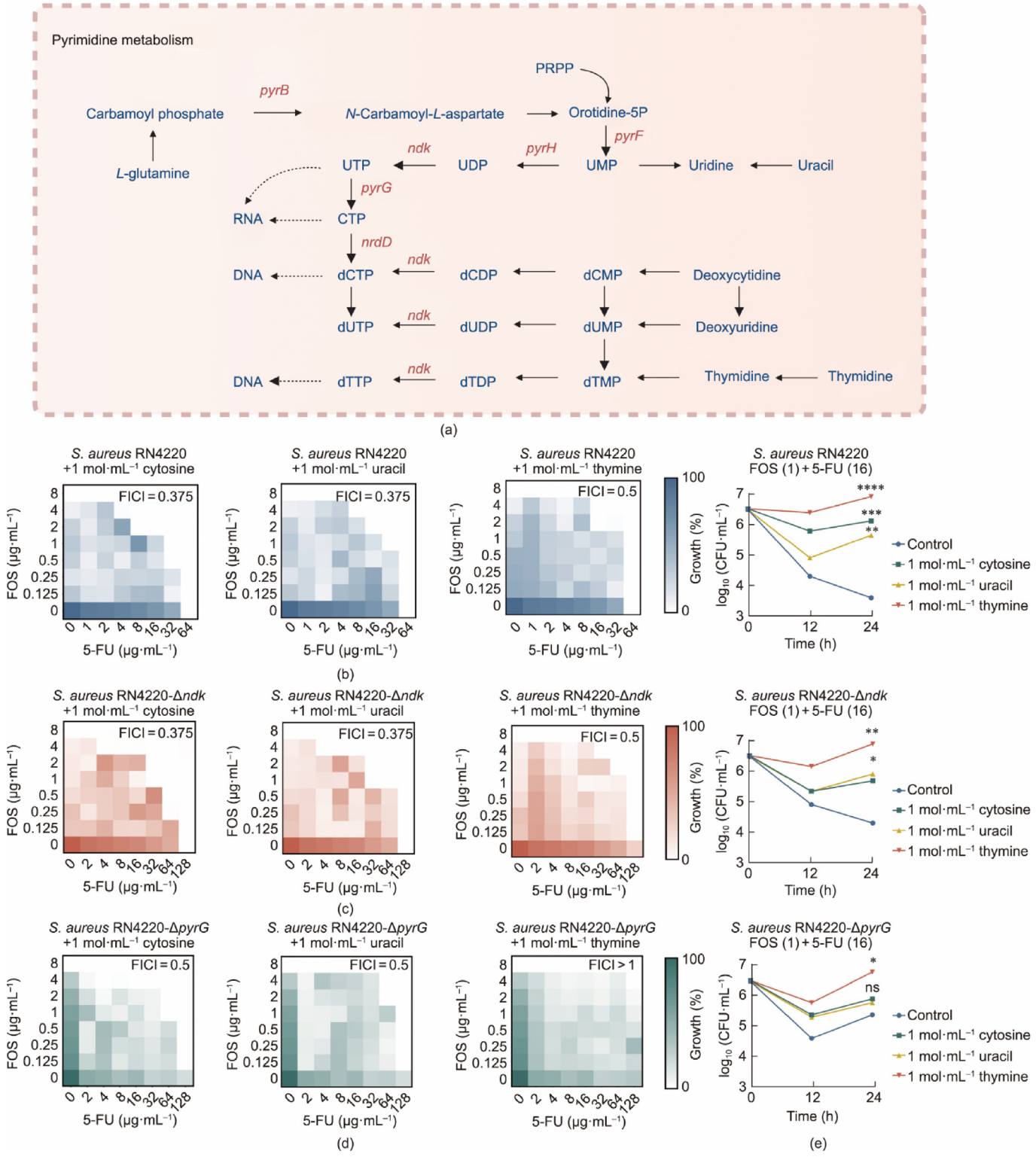

Fig. 4. Exogenous pyrimidine metabolites weaken the synergy between 5-FU and FOS. (a) Schematic diagram of the pyrimidine metabolic pathway. PRPP: phosphoribosyl pyrophosphate: UMP: uridine monophosphate; UDP: uridine diphosphate; UTP: uridine triphosphate; dCMP: deoxycytidine monophosphate; dCDP: deoxycytidine diphosphate; dCTP: deoxycytidine triphosphate; dUMP: deoxyuridine monophosphate; dUDP: deoxyuridine diphosphate; dUTP: deoxyuridine triphosphate; dTDP: deoxythymidine diphosphate; dTTP: deoxythymidine triphosphate. (b–d) Synergistic antibacterial effect of the 5-FU and FOS combination against (b) *S. aureus* RN4220, (c) *S. aureus* RN4220-Δ*ndk*, and (d) *S. aureus* RN4220-Δ*pyrG* with corresponding changes in CFU after the addition of cytosine, uracil, and thymine. (e) Time-killing curves of 5-FU and FOS after supplementation with pyrimidine metabolites. Data are shown as mean ± SD. *P* value was determined by unpaired *t*-test. $^{*}P < 0.05$, $^{**}P < 0.01$, $^{***}P < 0.001$, $^{****}P < 0.0001$, ns: not significant.

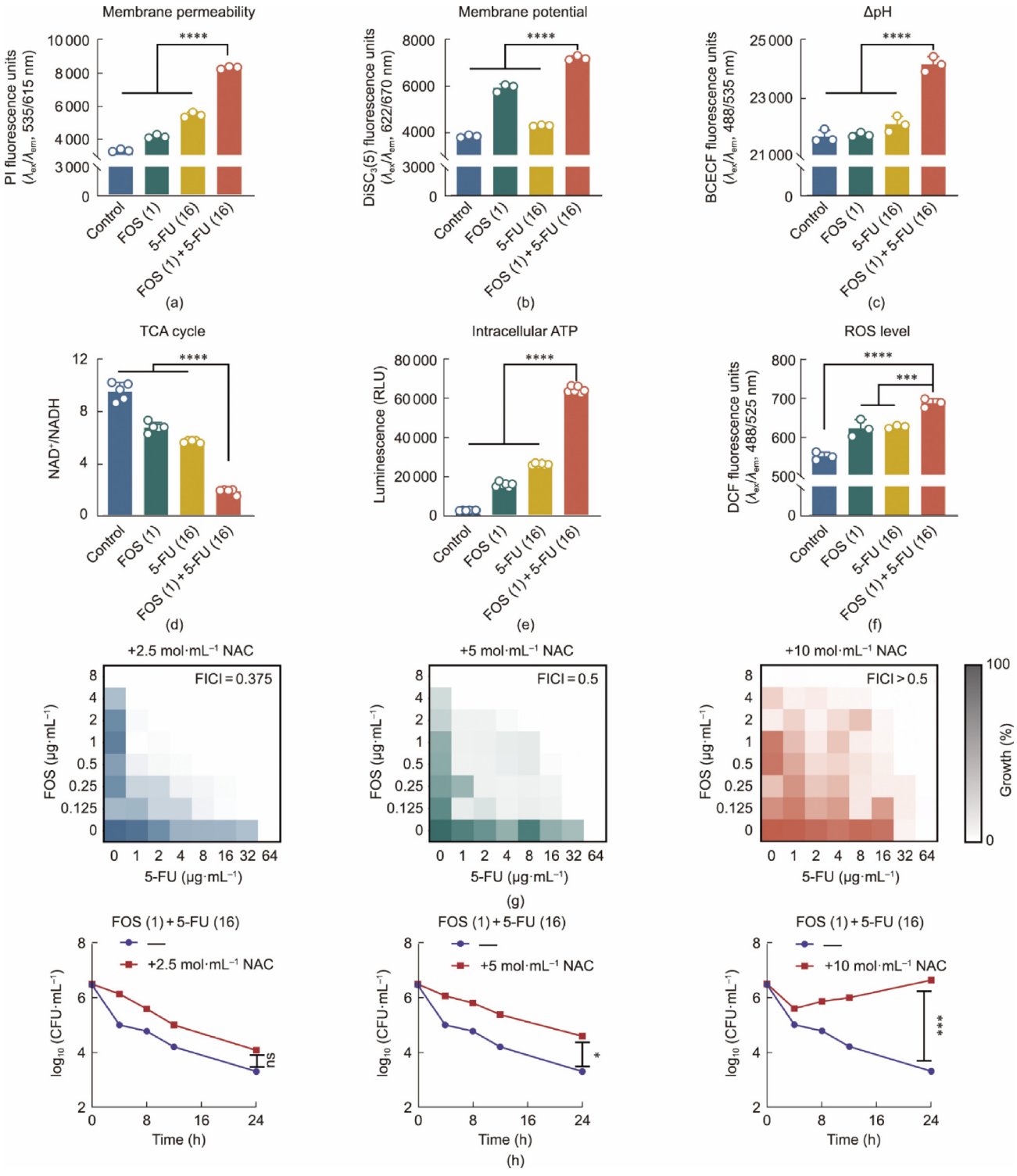

Fig. 5. The combination of 5-FU and FOS dissipates PMF and exacerbates oxidative damage. (a) Membrane permeability and (b) potential changes of MRSA T144 were altered following combined treatment of 5-FU and FOS. (c) Effect of the 5-FU and FOS combination on ΔpH in MRSA T144. (d) The NAD^+/NADH ratio in MRSA T144 after treatment with 5-FU and FOS, individually and in combination, is presented. (e) Intracellular ATP levels of MRSA T144 under various treatments, measured by monitoring the corresponding luminescence signals. (f) Intracellular ROS production in MRSA T144 was assessed. (g, h) The influence of exogenously added NAC (2.5, 5, and 10 mmol·L^{-1}) on their synergistic effect via checkerboard assays and time-killing curves. Data are shown as mean ± SD. *P* values in (a–e) were determined by one-way ANOVA or (h) *t*-test. $^*P < 0.05$, $^{***}P < 0.001$, $^{****}P < 0.0001$, ns: not significant.

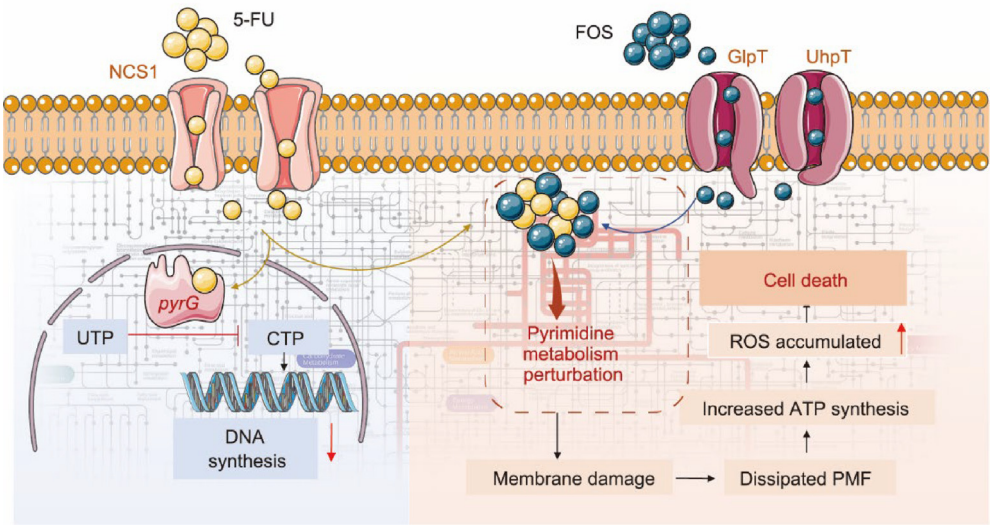

Fig. 6. Schematic diagram of the synergistic mechanism of the combination of 5-FU and FOS against MRSA. The 5-FU and FOS combination perturb bacterial pyrimidine metabolism, which causes membrane damage, PMF dissipation, elevated ATP and ROS production, ultimately leading to bacterial death. NCS1: neuronal calcium sensor 1; GlpT: glycolipid transfer protein; UhpT: sugar phosphate transporter.

< 0.0001) (Fig. 7(b)). Additionally, the *in vivo* efficacy of combination therapy was also confirmed in the mice peritonitis infection model, where the combination of FOS and 5-FU provided a survival benefit compared to the monotherapy group (P = 0.0071) (Fig. 7(c)). Bacterial loads measured in the organs of mice showed that the combination treatment group led to a reduction in CFU by 2–3 $\log_{10}$ compared to the monotherapy group (Fig. 7(d)). These encouraging results demonstrate the *in vivo* effectiveness of 5-FU and FOS combination for the treatment of MRSA-associated infections.

4. Discussion

The emergence and rapid spread of antibiotic resistance in pathogenic bacteria represent a global public health threat [51]. Identifying novel adjuvants to restore the efficacy of existing antibiotics offers a promising strategy for combating MDR bacteria, including MRSA [52]. Several studies have demonstrated the potential of antibiotic adjuvants, such as felodipine and diclofenac, to enhance the efficacy of antibiotics like aminoglycosides and β-lactams against drug-resistant strains [36,53]. Additionally, a growing body of research has explored alternatives to antibiotics, including antitoxins, antibodies, probiotics, and vaccines, as potential new therapeutic strategies [54–58]. However, many of these alternatives serve as adjunctive or preventative therapies, as their effectiveness as standalone treatments is still under investigation. In contrast, traditional antibiotics, particularly when combined with appropriate adjuvants, remain indispensable in the fight against resistant infections. Among these, FOS has regained attention due to its broad-spectrum activity, favorable safety profile, and its potential for synergism when combined with other agents such as polymyxins and linezolid [59,60]. In this study, we found that 5-FU, a chemotherapy drug, significantly enhanced the antibacterial effectiveness of FOS against MRSA infections. Meanwhile, our results indicated that a combination of 5-FU and FOS effectively inhibits biofilm formation and clears pre-formed biofilms, which are major contributors to chronic and recurrent infections [61,62].

CTP synthase, encoded by the *pyrG* gene, is a key enzyme in bacterial nucleotide metabolism, catalyzing the conversion of uridine triphosphate (UTP) to CTP, an essential precursor for RNA and DNA synthesis. This enzyme plays a pivotal role in maintaining the balance of the nucleotide pool, and its activity is tightly regulated by feedback mechanisms to ensure metabolic homeostasis [63]. Notably, our research revealed that 5-FU targets CTP synthase, thereby limiting CTP synthesis. This action imposes metabolic stress by perturbing the nucleotide biosynthesis equilibrium, sensitizing bacterial cells to further metabolic disturbances. Moreover, the inhibition of CTP synthase by 5-FU disrupted the entire pyrimidine metabolic pathway through complex feedback regulatory networks. This leads to significant changes in pyrimidine nucleotide synthesis and salvage pathways. Notably, there is a paradoxical increase in thymidine levels and a decrease in thymine levels. Accordingly, 5-FU inhibits dTMP synthesis and triggers compensatory thymidine salvage, partially restoring dTMP but exacerbating thymine depletion [64]. Mutations in *pyrG* amplify these responses [65], with *pyrG* mutant strains showing higher thymidine levels and more pronounced thymine depletion. This highlights the complexity of bacterial regulatory networks and the vulnerabilities in nucleotide metabolism that can be targeted for therapeutic intervention.

The metabolic disruption induced by 5-FU also uncovers its potential synergistic effects with existing antibiotics. Our study demonstrated that the combination of 5-FU and FOS disrupts pyrimidine biosynthesis by inhibiting DHODH, a key enzyme in the *de novo* pyrimidine synthesis pathway [66,67]. This inhibition not only reduced pyrimidine production but also dissipated bacterial PMF, leading to increased ATP synthesis and ROS accumulation. ROS-induced oxidative stress plays a central role in the bactericidal activity of this combination, as confirmed by the diminished effect upon the addition of ROS scavenger. These findings emphasize the therapeutic potential of combining 5-FU with FOS, highlighting the role of metabolic disturbance in enhancing antibiotic activity.

In conclusion, our study demonstrates that the combination of 5-FU and FOS effectively eradicates MRSA, as evidenced by both *in vitro* and *in vivo* models. Notably, we reveal that 5-FU could target bacterial CTP synthase. The combination of 5-FU and FOS perturbs pyrimidine metabolism, leading to bacterial membrane damage, PMF dissipation, enhanced ATP production, and increased oxidative damage. This cascade of metabolic disruption culminates in bacterial cell death, underscoring the importance of targeting critical metabolic pathways in potentiating antibiotic killing.

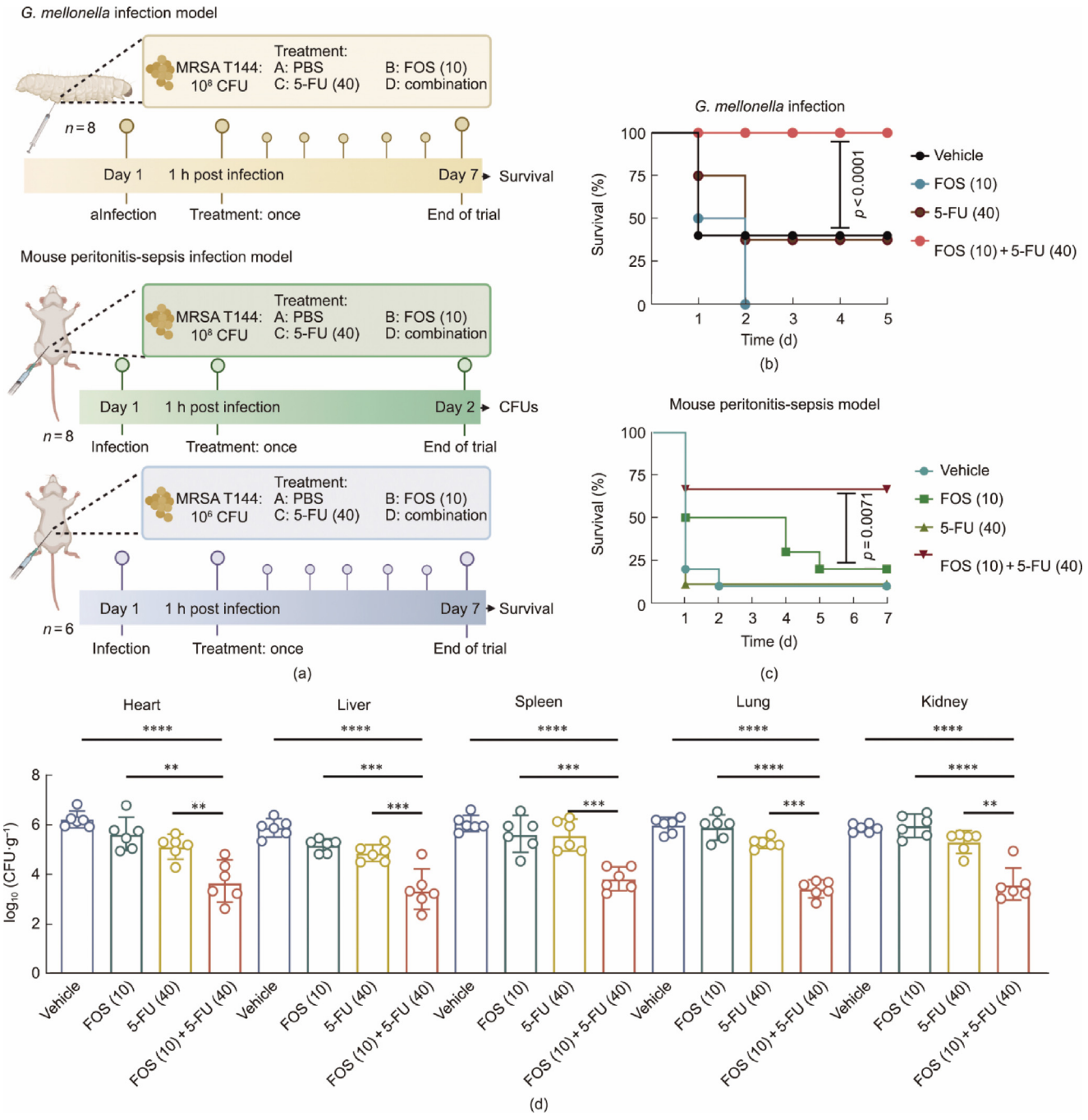

Fig. 7. *In vivo* efficacy of the 5-FU and FOS combination. (a) Schematic of the experimental design for the *G. mellonella* and murine peritonitis-sepsis infection models. (b, c) Survival curves of *G. mellonella* larvae and mice (n = 8 per group) infected with MRSA T144 and treated with the combination of 5-FU and FOS. P value was determined using a two-sided log-rank (Mantel-Cox) test. (d) Bacterial loads in the heart, liver, spleen, lungs, and kidneys of MRSA-infected mice subjected to different treatments regimens (n = 6 per group). Data are shown as adjusted P values were determined using two-way ANOVA with Sidak's multiple comparison test. $^{**}P < 0.01$, $^{***}P < 0.001$, $^{****}P < 0.0001$.

Together, these findings uncover the therapeutic promise of this combination as an effective strategy to combat MRSA infections and biofilm-associated persistence.

CRediT authorship contribution statement

Jianya Luo: Writing – original draft, Validation, Methodology. **Qingyan Lv:** Validation, Methodology. **Mengping He:** Validation, Methodology. **Zhiqiang Wang:** Funding acquisition, Conceptualization. **Yuan Liu:** Writing – review & editing, Project administration, Funding acquisition, Conceptualization.

Declaration of competing interest

All authors declare no conflict of interest.

Acknowledgments

This work was supported by the National Natural Science Foundation of China (32222084 and 32172907), the Key R&D Program of Jiangsu Province (Modern Agriculture) (BE2023332), the Jiangsu Agricultural Science and Technology Innovation Fund (CX(24)3072), the Project Funded by the Priority Academic Program Devel-

opment of Jiangsu Higher Education Institutions (PAPD), and 111 Project D18007.

Appendix A. Supplementary data

Supplementary data to this article can be found online at https://doi.org/10.1016/j.eng.2026.01.025.

References

[1] Lakhundi S, Zhang K. Methicillin-resistant *Staphylococcus aureus*: molecular characterization, evolution, and epidemiology. Clin Microbiol Rev 2018;31(4):e00020–118.
[2] Adedeji-Olulana AF, Wacnik K, Lafage L, Pasquina-Lemonche L, Tinajero-Trejo M, Sutton JAF, et al. Two codependent routes lead to high-level MRSA. Science 2024;386(6721):573–80.
[3] Yang R, Hou E, Cheng W, Yan X, Zhang T, Li S, et al. Membrane-targeting neolignan-antimicrobial peptide mimic conjugates to combat methicillin-resistant *Staphylococcus aureus* (MRSA) infections. J Med Chem 2022;65(24):16879–92.
[4] Rossolini GM, Arena F, Pecile P, Pollini S. Update on the antibiotic resistance crisis. Curr Opin Pharmacol 2014;18:56–60.
[5] Simard F, Gauthier C, Legault J, Lavoie S, Mshvildadze V, Pichette A. Structure elucidation of anti-methicillin resistant *Staphylococcus aureus* (MRSA) flavonoids from balsam poplar buds. Bioorg Med Chem 2016;24(18):4188–98.
[6] Borg MA, Camilleri L. What is driving the epidemiology of methicillin-resistant *Staphylococcus aureus* infections in Europe? Microb Drug Resist 2021;27(7):889–94.
[7] Bai AD, Lo CK, Komorowski AS, Suresh M, Guo K, Garg A, et al. *Staphylococcus aureus* bacteremia mortality across country income groups: a secondary analysis of a systematic review. Int J Infect Dis 2022;122:405–11.
[8] Sun H, Zhang Q, Wang R, Wang H, Wong YT, Wang M, et al. Resensitizing carbapenem- and colistin-resistant bacteria to antibiotics using auranofin. Nat Commun 2020;11(1):5263.
[9] Wang C, Xia Y, Wang R, Li J, Chan CL, Kao RY, et al. Metallo-sideromycin as a dual functional complex for combating antimicrobial resistance. Nat Commun 2023;14(1):5311.
[10] Toumi M, Rémuzat C. Value added medicines: what value repurposed medicines might bring to society? J Mark Access Health Policy 2017;5(1):1264717.
[11] Cacace E, Kim V, Varik V, Knopp M, Tietgen M, Brauer-Nikonow A, et al. Systematic analysis of drug combinations against Gram-positive bacteria. Nat Microbiol 2023;8(11):2196–212.
[12] Tyers M, Wright GD. Drug combinations: a strategy to extend the life of antibiotics in the 21st century. Nat Rev Microbiol 2019;17(3):141–55.
[13] Bollenbach T. Antimicrobial interactions: mechanisms and implications for drug discovery and resistance evolution. Curr Opin Microbiol 2015;27:1–9.
[14] Theuretzbacher U, Van Bambeke F, Cantón R, Giske CG, Mouton JW, Nation RL, et al. Reviving old antibiotics. J Antimicrob Chemother 2015;70(8):2177–81.
[15] Falagas ME, Vouloumanou EK, Samonis G, Vardakas KZ. Fosfomycin. Clin Microbiol Rev 2016;29(2):321–47.
[16] Kaye KS, Gales AC, Dubourg G. Old antibiotics for multidrug-resistant pathogens: from *in vitro* activity to clinical outcomes. Int J Antimicrob Agents 2017;49(5):542–8.
[17] Cohen SS, Flaks JG, Barner HD, Loeb MR, Lichtenstein J. The mode of action of 5-fluorouracil and its derivatives. Proc Natl Acad Sci USA 1958;44(10):1004–12.
[18] Kim W, Zhu W, Hendricks GL, Van Tyne D, Steele AD, Keohane CE, et al. A new class of synthetic retinoid antibiotics effective against bacterial persisters. Nature 2018;556(7699):103–7.
[19] Walz JM, Avelar RL, Longtine KJ, Carter KL, Mermel LA, Heard SO, et al. Anti-infective external coating of central venous catheters: a randomized, noninferiority trial comparing 5-fluorouracil with chlorhexidine/silver sulfadiazine in preventing catheter colonization. Crit Care Med 2010;38(11):2095–102.
[20] Zuo J, Quan Y, Li J, Li Y, Song D, Li X, et al. Tackling antibiotic resistance: exploring 5-fluorouracil as a promising antimicrobial strategy for the treatment of *Streptococcus suis* infection. Animals 2024;14(9):1286.
[21] Gieringer JH, Wenz AF, Just HM, Daschner FD. Effect of 5-fluorouracil, mitoxantrone, methotrexate, and vincristine on the antibacterial activity of ceftriaxone, ceftazidime, cefotiam, piperacillin, and netilmicin. Chemotherapy 1986;32(5):418–24.
[22] Nyhlén A, Ljungberg B, Nilsson-Ehle I, Odenholt I. Bactericidal effect of combinations of antibiotic and antineoplastic agents against *Staphylococcus aureus* and *Escherichia coli*. Chemotherapy 2002;48(2):71–7.
[23] Hussain M, Collins C, Hastings JG, White PJ. Radiochemical assay to measure the biofilm produced by coagulase-negative staphylococci on solid surfaces and its use to quantitate the effects of various antibacterial compounds on the formation of the biofilm. J Med Microbiol 1992;37(1):62–9.
[24] Attila C, Ueda A, Wood TK. 5-Fluorouracil reduces biofilm formation in *Escherichia coli* K-12 through global regulator AriR as an antivirulence compound. Appl Microbiol Biotechnol 2009;82(3):525–33.
[25] Zhang M, Yang S, Liu Y, Zou Z, Zhang Y, Tian Y, et al. Anticancer agent 5-fluorouracil reverses meropenem resistance in carbapenem-resistant Gram-negative pathogens. Int J Antimicrob Agents 2024;64(5):107337.
[26] Liu Y, Jia Y, Yang K, Li R, Xiao X, Zhu K, et al. Metformin restores tetracyclines susceptibility against multidrug resistant bacteria. Adv Sci 2020;7(12):1902227.
[27] Stokes JM, Yang K, Swanson K, Jin W, Cubillos-Ruiz A, Donghia NM, et al. A deep learning approach to antibiotic discovery. Cell 2020;180(4):688–702.
[28] Zhang S, Tang H, Wang Y, Nie B, Yang H, Yuan W, et al. Antibacterial and antibiofilm effects of flufenamic acid against methicillin-resistant *Staphylococcus aureus*. Pharmacol Res 2020;160:105067.
[29] Le P, Kunold E, Macsics R, Rox K, Jennings MC, Ugur I, et al. Repurposing human kinase inhibitors to create an antibiotic active against drug-resistant *Staphylococcus aureus*, persisters and biofilms. Nat Chem 2020;12(2):145–58.
[30] de Breij A, Riool M, Kwakman PH, de Boer L, Cordfunke RA, Drijfhout JW, et al. Prevention of *Staphylococcus aureus* biomaterial-associated infections using a polymer-lipid coating containing the antimicrobial peptide OP-145. J Control Release 2016;222:1–8.
[31] Silva ON, Torres MDT, Cao J, Alves ESF, Rodrigues LV, Resende JM, et al. Repurposing a peptide toxin from wasp venom into antiinfectives with dual antimicrobial and immunomodulatory properties. Proc Natl Acad Sci USA 2020;117(43):26936–45.
[32] Ling LL, Schneider T, Peoples AJ, Spoering AL, Engels I, Conlon BP, et al. A new antibiotic kills pathogens without detectable resistance. Nature 2015;517(7535):455–9.
[33] Antipov D, Korobeynikov A, McLean JS, Pevzner PA. HybridSPAdes: an algorithm for hybrid assembly of short and long reads. Bioinformatics 2016;32(7):1009–15.
[34] Cai J, Shi J, Chen C, He M, Wang Z, Liu Y. Structural-activity relationship-inspired the discovery of saturated fatty acids as novel colistin enhancers. Adv Sci 2023;10(29):e2302182.
[35] Chen W, Zhang Y, Yeo WS, Bae T, Ji Q. Rapid and efficient genome editing in *Staphylococcus aureus* by using an engineered CRISPR/Cas9 system. J Am Chem Soc 2017;139(10):3790–5.
[36] Zhang S, Qu X, Jiao J, Tang H, Wang M, Wang Y, et al. Felodipine enhances aminoglycosides efficacy against implant infections caused by methicillin-resistant *Staphylococcus aureus*, persisters and biofilms. Bioact Mater 2022;14:272–89.
[37] Livak KJ, Schmittgen TD. Analysis of relative gene expression data using real-time quantitative PCR and the $2(-\Delta\Delta C(T))$ method. Methods 2001;25(4):402–8.
[38] Liu Y, Shi J, Tong Z, Jia Y, Yang K, Wang Z. Potent broad-spectrum antibacterial activity of amphiphilic peptides against multidrug-resistant bacteria. Microorganisms 2020;8(9):1398.
[39] Heidelberger C, Chaudhuri NK, Danneberg P, Mooren D, Griesbach L, Duschinsky R, et al. Fluorinated pyrimidines, a new class of tumour-inhibitory compounds. Nature 1957;179(4561):663–6.
[40] Mao C, Xiang Y, Liu X, Zheng Y, Yeung KWK, Cui Z, et al. Local photothermal/photodynamic synergistic therapy by disrupting bacterial membrane to accelerate reactive oxygen species permeation and protein leakage. ACS Appl Mater Interfaces 2019;11(19):17902–14.
[41] Jia Y, Yang B, Shi J, Fang D, Wang Z, Liu Y. Melatonin prevents conjugative transfer of plasmid-mediated antibiotic resistance genes by disrupting proton motive force. Pharmacol Res 2022;175:105978.
[42] Zhang H, Chen Q, Xie J, Cong Z, Cao C, Zhang W, et al. Switching from membrane disrupting to membrane crossing, an effective strategy in designing antibacterial polypeptide. Sci Adv 2023;9(4):eabn0771.
[43] Kumar A, Boradia VM, Thakare R, Singh AK, Gani Z, Das S, et al. Repurposing ethyl bromopyruvate as a broad-spectrum antibacterial. J Antimicrob Chemother 2019;74(4):912–20.
[44] Yssel AEJ, Vanderleyden J, Steenackers HP. Repurposing of nucleoside- and nucleobase-derivative drugs as antibiotics and biofilm inhibitors. J Antimicrob Chemother 2017;72(8):2156–70.
[45] Fang J, Uchiumi T, Yagi M, Matsumoto S, Amamoto R, Takazaki S, et al. Dihydro-orotate dehydrogenase is physically associated with the respiratory complex and its loss leads to mitochondrial dysfunction. Biosci Rep 2013;33(2):e00021.
[46] Farha MA, Verschoor CP, Bowdish D, Brown ED. Collapsing the proton motive force to identify synergistic combinations against *Staphylococcus aureus*. Chem Biol 2013;20(9):1168–78.
[47] Lobritz MA, Belenky P, Porter CB, Gutierrez A, Yang JH, Schwarz EG, et al. Antibiotic efficacy is linked to bacterial cellular respiration. Proc Natl Acad Sci USA 2015;112(27):8173–80.
[48] Liu Y, Yang K, Jia Y, Shi J, Tong Z, Wang Z. Thymine sensitizes Gram-negative pathogens to antibiotic killing. Front Microbiol 2021;12:622798.
[49] Imlay JA. The molecular mechanisms and physiological consequences of oxidative stress: lessons from a model bacterium. Nat Rev Microbiol 2013;11(7):443–54.
[50] Halasi M, Wang M, Chavan TS, Gaponenko V, Hay N, Gartel AL. ROS inhibitor *N*-acetyl-$_L$-cysteine antagonizes the activity of proteasome inhibitors. Biochem J 2013;454(2):201–8.
[51] Boucher HW, Talbot GH, Bradley JS, Edwards JE, Gilbert D, Rice LB, et al. Bad bugs, no drugs: no ESKAPE! An update from the infectious diseases society of America. Clin Infect Dis 2009;48(1):1–12.
[52] Melander RJ, Melander C. The challenge of overcoming antibiotic resistance: an adjuvant approach? ACS Infect Dis 2017;3(8):559–63.
[53] Zhang S, Qu X, Tang H, Wang Y, Yang H, Yuan W, et al. Diclofenac resensitizes methicillin-resistant *Staphylococcus aureus* to β-lactams and prevents implant infections. Adv Sci 2021;8(13):2100681.

[54] Czaplewski L, Bax R, Clokie M, Dawson M, Fairhead H, Fischetti VA, et al. Alternatives to antibiotics—a pipeline portfolio review. Lancet Infect Dis 2016;16(2):239–51.
[55] Johnson BK, Abramovitch RB. Small molecules that sabotage bacterial virulence. Trends Pharmacol Sci 2017;38(4):339–62.
[56] Dickey SW, Cheung GYC, Otto M. Different drugs for bad bugs: antivirulence strategies in the age of antibiotic resistance. Nat Rev Drug Discov 2017;16(7):457–71.
[57] DiGiandomenico A, Sellman BR. Antibacterial monoclonal antibodies: the next generation? Curr Opin Microbiol 2015;27:78–85.
[58] Skeiky YA, Sadoff JC. Advances in tuberculosis vaccine strategies. Nat Rev Microbiol 2006;4(6):469–76.
[59] Chi J, Li Y, Zhang N, Liu H, Chen Z, Li J, et al. Fosfomycin enhances the inhibition ability of linezolid against biofilms of vancomycin-resistant *Enterococcus faecium* in vitro. Infect Drug Resist 2023;16:7707–19.
[60] Ribeiro ACDS, Chikhani YCDSA, Valiatti TB, Valêncio A, Kurihara MNL, Santos FF, et al. *In vitro* and *in vivo* synergism of fosfomycin in combination with meropenem or polymyxin B against KPC-2-producing *Klebsiella pneumoniae* clinical isolates. Antibiotics 2023;12(2):237.
[61] Yan J, Bassler BL. Surviving as a community: antibiotic tolerance and persistence in bacterial biofilms. Cell Host Microbe 2019;26(1):15–21.
[62] Defraine V, Fauvart M, Michiels J. Fighting bacterial persistence: current and emerging anti-persister strategies and therapeutics. Drug Resist Updat 2018;38:12–26.
[63] Rao Y, Qin C, Savas AC, Liu Q, Feng S, Hou G, et al. Pyrimidine synthesis enzyme CTP synthetase 1 suppresses antiviral interferon induction by deamidating IRF3. Immunity 2025;58(1):74–89.
[64] Oe C, Hayashi H, Hirata K, Kawaji K, Hashima F, Sasano M, et al. Pyrimidine analogues as a new class of Gram-positive antibiotics, mainly targeting thymineless-death related proteins. ACS Infect Dis 2020;6(6):1490–500.
[65] Zheng YD, Zhong T, Wu H, Li N, Fang Z, Cao L, et al. Crizotinib shows antibacterial activity against Gram-positive bacteria by reducing ATP production and targeting the CTP synthase PyrG. Microbiol Spectr 2022;10(3):e0088422.
[66] West TP. Pyrimidine nucleotide synthesis in *Pseudomonas nitroreducens* and the regulatory role of pyrimidines. Microbiol Res 2014;169(12):954–8.
[67] Lane AN, Fan TW. Regulation of mammalian nucleotide metabolism and biosynthesis. Nucleic Acids Res 2015;43(4):2466–85.